Soft Matter

Accepted Manuscript

ROYAL SOCIETY OF CHEMISTRY

www.rsc.org/softmatter

Hydration lubrication and shear-induced self-healing of lipid bilayer boundary lubricants in phosphatidylcholine dispersions.

Raya Sorkin[1], Nir Kampf[1], Linyi Zhu[1,2] and Jacob Klein[1]

1.Weizmann Institute of Science, Materials and interfaces department, Rehovot, Israel

2. Key Laboratory of Colloid and Interface Science, Beijing National Laboratory for Molecular Sciences (BNLMS), Institute of Chemistry, Chinese Academy of Sciences, Beijing 100190, P.R. China

Abstract

Measurements of normal and shear (frictional) forces between mica surfaces across small unilamellar vesicle (SUV) dispersions of the phosphatidylcholine (PC) lipids DMPC (14:0), DPPC (16:0) and DSPC (18:0) and POPC (16:0, 18:1), at physiologically high pressures, are reported. We have previously studied the normal and shear forces between two opposing surfaces bearing PC vesicles across pure water and showed that liposome lubrication ability improved with increasing acyl chain length, and correlated strongly with the SUV structural integrity on the substrate surface (DSPC>DPPC>DMPC). In the current study, surprisingly, we discovered that this trend is reversed when the measurements are conducted in SUV dispersions, instead of pure water. In their corresponding SUV dispersion, DMPC SUVs ruptured and formed bilayers, which were able to provide reversible and reproducible lubrication with extremely low friction ($\mu<10^{-4}$) up to pressures of 70-90 atm. Similarly, POPC SUVs also formed bilayers which exhibited low friction ($\mu<10^{-4}$) up to pressures as high as 160 atm. DPPC and DSPC SUVs also provided good lubrication, but with slightly higher friction coefficients ($\mu=10^{-3}$-10^{-4}). We believe these differences originate from fast self-healing of the softer surface layers (which are in their liquid disordered phase, POPC, or close to it, DMPC), which renders the robustness of the DPPC or DSPC (both in their solid ordered phase) less important at these conditions. Under these circumstances, the enhanced hydration of the less densely packed POPC and DMPC surface layers is now believed to play an important role, and allows enhanced lubrication via the hydration lubrication mechanism. Our findings may have implications for the understanding of complex biological systems such us biolubrication of synovial joints.

Introduction

Lipids have myriad physiological roles [1], including contributing to the remarkable lubrication capabilities of synovial joints [2-13]. Several mechanisms have been proposed in order to explain the very efficient physiological lubrication, characterized by friction coefficients μ in the range 0.001-0.01 [14, 15]. Under conditions of low velocities and high contact pressures, (local pressures in synovial joints can reach 180 atm [16, 17]) the prevailing lubrication mechanism is believed to be that of boundary lubrication [3, 18-29]. In this mechanism, surface-attached molecules (rather than trapped fluid, as in e.g hydrodynamic lubrication mechanism) provide lubrication as the sliding surfaces come into contact at their asperities. Different macromolecules, including lipids, have been proposed to function as boundary lubricants at the cartilage surface [14, 19, 20, 24, 25, 27, 30-34]. Phospholipids PLs were originally conjectured to provide lubrication by sliding between the exposed alkyl chains at the surfaces [3], as in the classical boundary lubrication mode of machine tribology [35, 36]. However, more recent work demonstrated that such systems provide lubrication via the hydration lubrication mechanism, enabled by the hydration layers of the phosphocholine head groups of the lipids [13, 32, 37-41].

While lipids are clearly present on the cartilage surface [19, 42] and in the synovial fluid [3, 21, 43] and they are capable of providing highly efficient lubrication at physiologically high pressures [32, 37, 38, 40, 44], the exact configuration of lipid species on the cartilage surface and its possible dynamical remodeling remains unclear. Lipids were reported in vivo on the cartilage surface possibly as multilayers [2] and as vesicles [45]. The difficulty to analyze the cartilage surface results from the changes it undergoes once extracted from the physiological environment [9]. Both its chemical composition and morphology may change upon removal [46], most likely due to the enzymatic degradation of macromolecules following the trauma suffered by the tissue [47, 48]. Nonetheless, nanotribology of molecular components of synovial joints has led to advances in our understanding [29]. A recent proposal [13], relevant to the present study, holds that there is a synergistic effect between various molecules present on the cartilage surface, including in particular lipids, and that macromolecular species present in the superficial zone of the cartilage are forming complexes with lipids, or otherwise contributing to their stability (e.g. refs. [13, 32, 49, 50] and references therein). This study [13], where friction between mica surfaces bearing boundary layers consisting of a complex of hyaluronan and PC lipids was measured in a Surface Force Balance (SFB), showed that such layers could provide physiologically low values of the friction ($\mu \approx 10^{-3}$) at physiologically-high contact pressures (of order 100 atm).

While the surface of mica is very different from that of cartilage, boundary friction measured in the SFB arises from dissipation at the slip plane between the boundary layers which come into direct contact. It is thus characteristic of the boundary layers themselves rather than of the underlying mica substrates [14, 29]. Soft surfaces, such as cartilage, deform at the physiological pressures in joints, flattening their asperities, to contact each other intimately over their compressed area. In this case also the surface-attached molecules forming the boundary layers, rather than the underlying cartilage surfaces, are at the interface where frictional energy is dissipated; thus the model system of mica-supported surface layers in the SFB is believed to be relevant also for physiological systems.

We have previously studied in detail [41] the normal and shear forces between two mica surfaces bearing adsorbed lipids or layers of small unilamellar vesicles (SUVs) across pure water. We examined SUVs composed of phosphatidylcholine lipids (PCs), with different di-acyl chain lengths: 14:0 (DMPC), 16:0 (DPPC) and 18:0 (DSPC), revealing substantial differences in their lubrication capabilities. (X:Y notation indicates the number of carbons in the fatty acid chains and the degree of unsaturation, respectively.) When the PC-SUVs were adsorbed to mica surfaces, which were then rinsed and studied across lipid-free water in the SFB, the lubrication performance improved with the increase in the acyl chain length. We found correlation between the lubrication efficiency and the structure of the lipids on the mica surface, as DSPC liposomes were more robust and able to maintain their vesicular structure, while DPPC were marginally stable, and DMPC liposomes ruptured spontaneously upon adsorption to the mica surface and formed continuous bilayers. The main Solid-Ordered to Liquid-Disordered (SO-to-LD) transition temperatures of unsupported bilayers of these PCs are 24^0C, 41^0C and 54^0C respectively [51]. We observed that as the lipids move deeper into the SO phase, corresponding to longer acyl tails - and thus stronger hydrophobic interactions between them – the SUVs robustness on the mica surface is increased [41]. At the same time, an early study of a rinsed POPC liposome layer (in pure water) showed poor lubrication ability which was also attributed to reduced mechanical stability of the LD-phase vesicles [38]. It appears, therefore, that under these conditions where SUVs were interacting across a liposome-free aqueous medium, the mechanical stability to compression and shear of the surface-attached, close-packed liposomes was an important factor in their lubrication ability (together with their closed vesicular and correspondingly more defect-free nature [40, 41].

In the current study, we extend our previous work carried out in lipid-free water [41] to examine the lubrication performance of the same series of PC-SUVs (14:0, 16:0, 18:0), and in addition the (16:0, 18:1) POPC-SUV, across the respective SUV dispersions - in other words, under conditions where there is a lipid/liposome reservoir in contact with the surfaces. POPC is added as an extreme case, as the transition temperature for this lipid is -2ºC due to a kink in the unsaturated oleoyl chain which hinders chain packing. We measure the normal and shear forces for these systems using the SFB, and also examine the effect of rubbing DMPC bilayers with an AFM tip on the surface morphology. In these conditions, the lipids in solution are at their saturated concentration, pinned at the respective c.m.c's, henceforth designated 'saturated solutions'. One motivation for the study of lubrication across liposome dispersions is that such dispersions provide a reservoir of lipids, conditions which may better resemble physiological conditions, as there is now evidence that different physiological fluids [52-54], including the synovial fluid [55], contain lipids or lipid vesicles. Moreover, many cell types secrete extracellular vesicles (EVs), exosomes and microvesicles, which play significant physiological roles [52-54]. As lipids are present both in the synovial fluid as well as on the cartilage surface [19, 43], it is possible that a lipid reservoir may contribute to the stability of surface attached lipid layers, and thus may play a role in their function as boundary lubricants.

Materials and Methods

Materials

The lipids, 1-palmitoyl-2-oleoyl-*sn*-glycero-3-phosphocholine (POPC, 16:0-18:1) 1,2-dimyristoyl-*sn*-glycero-3-phosphatidylcholine (DMPC,14:0), 1,2-dipalmitoyl-*sn*-glycero-3 phosphatidylcholine (DPPC 16:0) and 1,2-distearoyl-*sn*-glycero-3- phosphatidylcholine (DSPC, 18:0), were purchased from Lipoid (Ludwigshafen, Germany). The main SO-to-LD transition temperatures of unsupported bilayers of these PCs are -2^0C, 24^0C, 41^0C and 54^0C respectively [51]. Ultrapure (conductivity) water was obtained by treating tap water with an activated charcoal filter followed by a Barnstead NanoPure system. The water specific resistivity was 18.2 MΩ and the concentration of total organic compounds (TOC) was below 1ppb. The mica was ruby muscovite, grade 1, supplied by S&J Trading Inc., NY. Shell "EPON 1004" resin was used to glue the mica sheets to the quartz lenses.

Liposome preparation

Single unilamellar vesicles (SUVs) were prepared using standard approaches [38, 56]. Briefly, lipids were dispersed in water, ultra-sonicated for 5 min and homogenized for 5 min at the appropriate temperature above the main phase transition of each lipid in order to obtain

dispersed multilamellar vesicles (MLV). Next, the MLVs were progressively downsized using an extruder (Northern lipid Inc, Burnaby, BC, Canada) through polycarbonate filters having defined pore sizes starting with 400nm (3 cycles), 100nm (4 cycles) and ending with 50nm (10 cycles). Liposomal size distribution (by volume) was determined in pure water using a Viscotek 802 DLS. The average diameter for all liposome preparations used was 60 ±15 nm. Subsequent to their adsorption on the surface, samples were also characterized by AFM. For both AFM scans and SFB measurements, freshly cleaved mica (mounted on cylindrical lenses for use in the SFB, see below) was placed in a 0.3 mM SUV dispersion prepared with Barnstead NanoPure purified conductivity water. Measurements were conducted starting from 30min following addition of the liposome dispersion. The mica surfaces in each case were immersed in the SUV dispersion added to the SFB bath, in which measurements were carried out. The bath volume was 12ml.

Atomic force microscopy (AFM)

Imaging of surfaces and nanomechanical measurements were carried out with an MFP-3D SA (AFM) instrument (Asylum Research, Santa Barbara, CA). Scanning in tapping mode in conductivity water was conducted using a silicon nitride V-shaped 115μm long cantilever having a nominal spring constant of 0.35 N/m with a pyramidal silicon tip with a nominal radius of 2nm (SNL, Bruker).

Surface Force Balance (SFB)

The procedures of the mica- SFB technique has been described in detail previously [57]. Briefly, the measurement of normal (F_n) and shear (F_s) forces was conducted between two curved, back-silvered, atomically-smooth mica surfaces, in a crossed-cylinder configuration (mean radius of curvature, R), by monitoring the bending of two orthogonal leaf springs, a vertical spring and a horizontal spring (a schematic is shown in the inset to figure 1). The bending of the horizontal spring is determined using multiple beam interferometry; the separation of closest approach, D, is optimally measured to ±2-3Å by monitoring the wavelength of optical interference fringes of equal chromatic order (FECO). The bending of the vertical springs which provides a direct measure of the shear forces is monitored by an air-gap capacitor.

Normal force profiles $F_n(D)/R$ and shear traces $F_s(t)$ were recorded in the same approach and separation cycles, as the surfaces were progressively compressed ($F_n(D)/R$ is, in the Derjaguin

approximation, proportional to the interaction energy per unit area between two flat parallel surfaces obeying the same force law, and is a means of normalizing results obtained using different curvature surfaces [58]). At each surface separation, both during compression and upon separation of the surfaces, shear motion was applied for one minute (and sometimes for one hour to examine the effect of prolonged shear). Shear profiles were taken by directly measuring the response of the lower surface to lateral motion applied to the upper surface. Lateral amplitudes (applied by the PZT actuator), Δx_0, in the range of 200-1200 nm and shear velocities v_s in the range 10-600 nm/sec were applied. Shear force traces were measured simultaneously with normal force profiles by applying lateral motion at several separations at progressively increasing (or decreasing) the normal loads. Shear forces F_s are measured from the plateau regime of the friction-force vs. time traces (shown later), where F_s is independent of the shear amplitude. The magnitude of the weakest shear forces is determined either by filtering the signal about the drive frequency, or by fast Fourier transform of the data to yield F_s at the drive frequency, see e.g. refs. [59, 60]; the two approaches yield similar values of F_s. The results presented here are based on 6 independent experiments, each with at least three different contact points between the interacting surfaces, with several approach and retraction profiles at each contact point, carried out in temperature-stabilized rooms of 25±0.2ºC.

The normal compressive loads applied during the experiments cause an elastic flattening of the curved surfaces, of area A, due mostly to compression of the glue supporting the mica sheet. This is clearly observed as flattening of radius *a* (e.g in the inset to figure 2, showing flattening of a = 60μm) at the tips of the interference fringes. The mean pressure, P, between the compressed surfaces can be directly evaluated from the dimensions of this flattened area as $P=F_n/A= F_n/\pi a^2$. The flattening of contacting, non-adhering surfaces can be also evaluated from Hertzian contact mechanics [61], and can then be used for pressure evaluation. This method is preferred for cases of small flattening (small *a*). Detailed explanations of the mean pressure evaluation for similar SFB measurements are given elsewhere [41].

Results and discussion

From our previous studies in a lipid-free aqueous environment [40, 41], we know that DMPC SUVs fuse and form continuous bilayers upon their encounter with mica, whereas DPPC SUVs are marginally stable, and DSPC SUVs are stable and robust on the mica surface [41]. POPC-SUVs immersed in lipid-free water were found to collapse under pressure when adsorbed on mica [38] (and thus formed poor boundary lubricating layers). We now extend these studies of

the different lipids (POPC, DMPC, DPPC and DSPC) in pure (lipid-free) water to the case where the surface-immersion medium consists of the corresponding SUV dispersions.

Normal surface forces

In figure 1, normal force profiles $F_n(D)/R$ between mica surfaces across a POPC-SUV dispersion (0.3mM) are shown. No substantial long range forces are observed, (consistent with electrostatic double layer interactions in the salt-free medium [62]) while the final high-compression separation D = 9 ± 1 nm corresponds to the thickness of two bilayers [63], suggesting that bilayer covered surfaces are formed at these conditions. There little difference between first and subsequent approaches. In several cases (inset to figure 1) a final separation of 5±1 nm was recorded, most likely due to hemifusion, as observed previously for other bilayer systems [64].

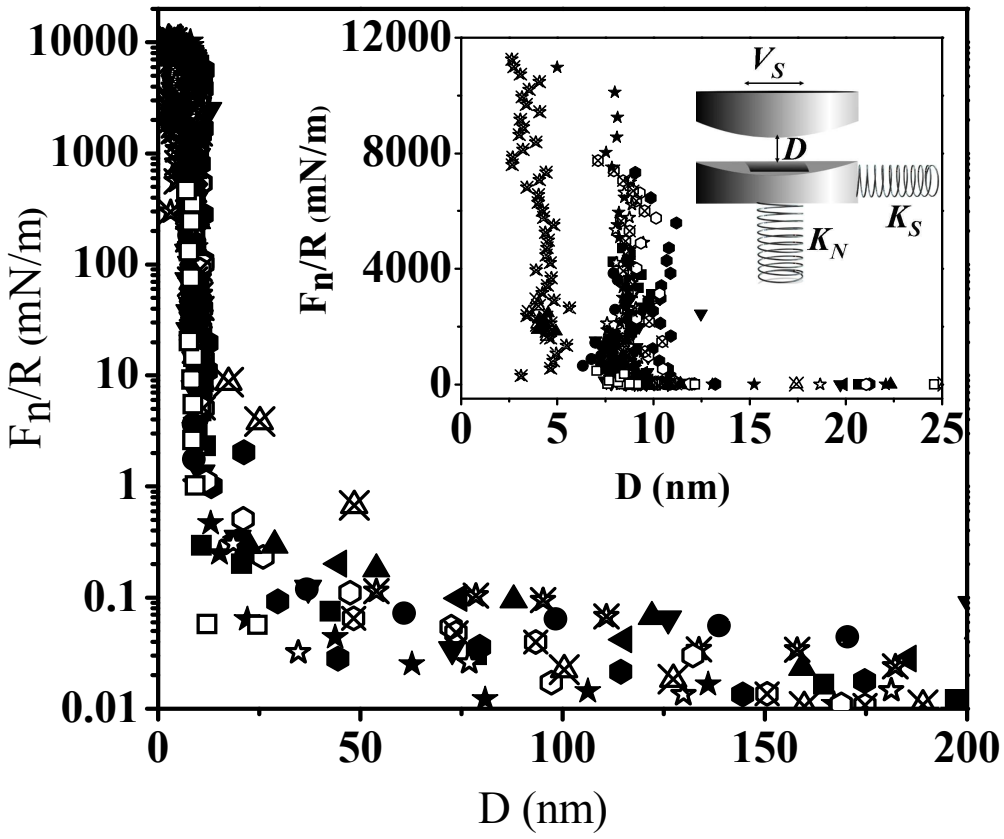

Figure 1: Force $F_n(D)$ versus distance D profiles between mica surfaces across POPC SUV dispersion normalized as $F_n(D)/R$. D = 0 separation is defined with respect to mica-mica contact in pure water. Filled symbols are first approaches, empty symbols are second approaches and crossed symbols correspond to force profiles taken on separation of the surfaces. Inset: shows the profiles on a magnified linear-linear scale. The final separation is

9±1 nm or 5±1 nm (see text). Also shown is a schematic representation of the SFB configuration.

In figure 2, normal force profiles between mica surfaces across a DMPC-SUV dispersion (0.3mM) are shown. For comparison, force profiles for the corresponding measurements between adsorbed and rinsed DMPC-SUVs across pure water, taken from ref [41], are shown in the shaded area. The force plots are within a comparable range; however, there is less scatter in the data across the DMPC dispersion. In this case, the strong repulsion commenced at D ≈ 14 nm, to a final (high compression) separation D= 8.5±1nm, corresponding to the thickness of two bilayers. The optical fringes at contact between the surfaces for this system are also shown in the inset to figure 2. Their smoothness is an indication to the uniformity and smoothness of the compressed DMPC bilayers (we note that for the POPC system too, similarly flat and uniform fringes (not shown) were observed). It is likely that DMPC liposomes from the dispersion adhere to the mica surfaces, and within a short time (as previously discussed [41]) fuse and form a continuous bilayer. First and second approaches to contact are reproducible (shear measurements are performed simultaneously with the normal forces) with no indications of either squeeze out or damage of the bilayer following first approach to contact.

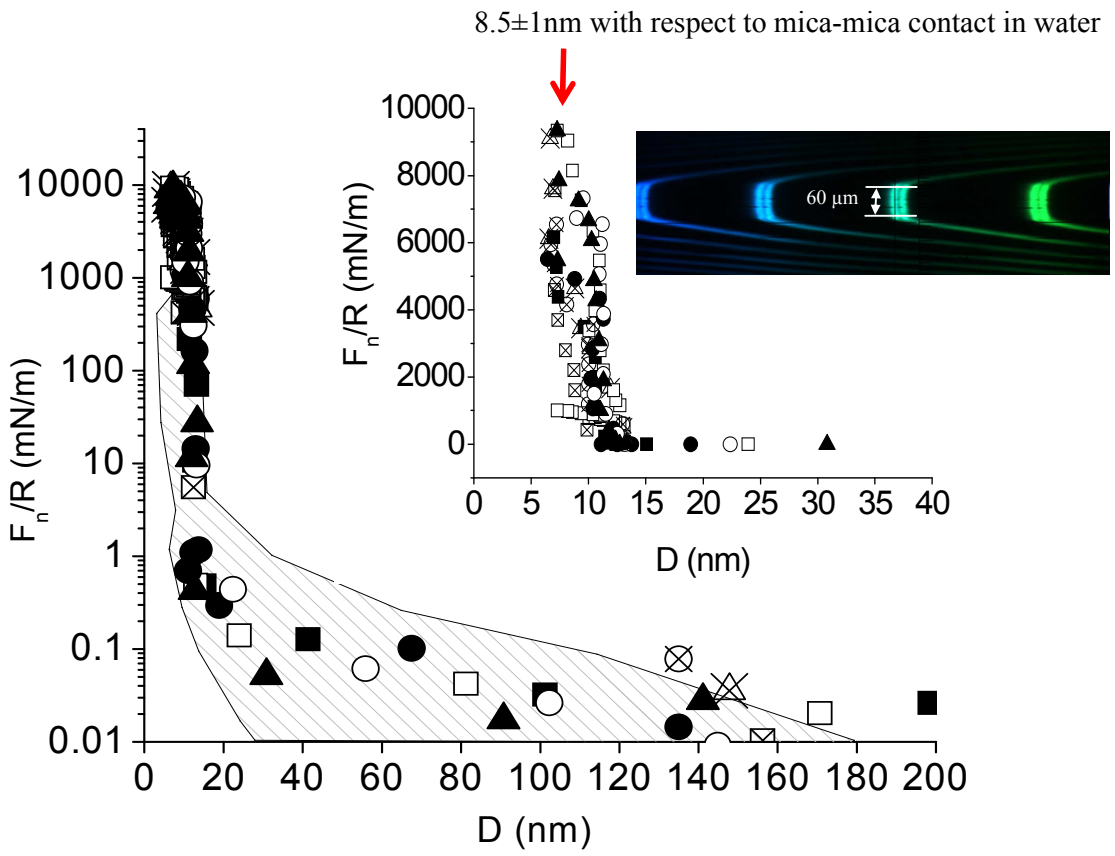

Figure 2: Force $F_n(D)$ versus distance D profiles between mica surfaces across DMPC SUV dispersion normalized as $F_n(D)/R$. D = 0 separation is defined with respect to mica-mica contact in air. Filled symbols are first approaches, empty symbols are second approaches and crossed symbols correspond to force profiles taken on separation of the surfaces. Inset: shows the profiles on a magnified linear-linear scale, and the image of optical fringes at contact, at a pressure of 80atm. Shaded area indicates the range of force profiles for DMPC bilayers in pure water, as described in [41]

A very different behavior was observed for the DPPC SUVs system, as shown in figure 3. For this system, significant repulsion forces (>1 mN/m) commence already at ca. 100nm (unlike POPC and DMPC where such forces are observed only below ca. 40nm, figures 1, 2). From the DLS measurements, the DPPC liposome diameter is 50±10nm. Thus, adsorption of a single layer of unperturbed liposomes to each surface would result in a separation at onset of steric repulsion at D ≈ 100nm. As it is known that liposomes flatten upon adsorption [38, 65-67], the onset of repulsion forces at D ≈ 100nm in fact most likely corresponds to a flattened SUV layer with an overlayer of loosely attached SUVs, as previously observed [38, 41]. Then, upon further compression, the repulsion increases as the excess SUV layers are squeezed out and the SUVs in contact with the mica surfaces are further flattened, losing their water content. A

"hard wall" is reached at D = 18±1 nm, roughly corresponding to 2 bilayers on each surface; however, upon further compression the surfaces abruptly jump to D = 8.5±1.5 nm. This jump can be readily seen in the inset of figure 3. In some profiles, even at such pressure this inward jump did not occur, and the final separation of 17±1 was measured. The change in the separation from D 18±1 nm to D ≈ 8.5 nm suggests that each flattened SUV layer (two bilayers) ruptures to form a single continuous bilayer, while the excess material (one bilayer from each surface) is squeezed out. It should be noted that subsequent approaches to contact come directly to a final separation D = 8.5±1.5 nm (with no jump-in, as on first approach, from D ≈ 18 nm), which indicates stable attachment of the bilayers to the mica surface, and no detachment or further adsorption of additional lipids or liposomes from the dispersion.

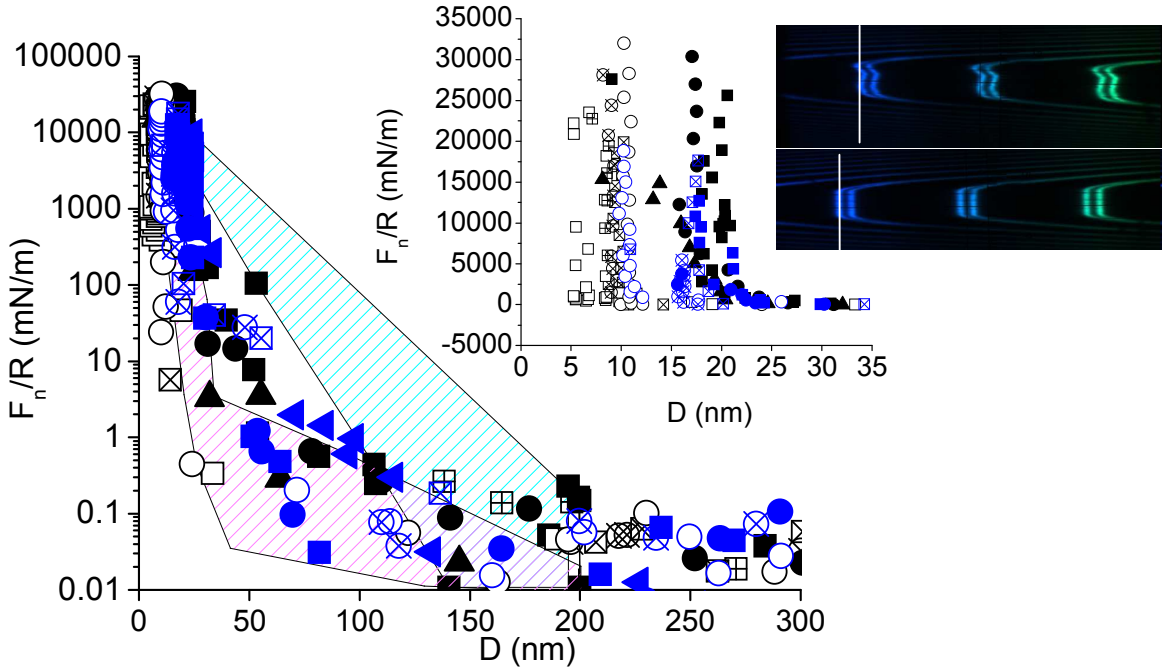

Figure 3: Force $F_n(D)$ versus distance D profiles between mica surfaces across DPPC SUV dispersion normalized as $F_n(D)/R$. D = 0 separation is defined with respect to air calibration. Filled symbols are first approaches, empty symbols are second approaches and crossed symbols correspond to force profiles taken on separation of the surfaces. Inset: shows the profiles on a magnified linear-linear scale, final separation 10±1 nm, and the image of optical fringes taken at pressures of 130 atm (top) and 147 atm (bottom). White vertical lines are a guide to the eye to follow change in fringe position. Red and blue shaded areas indicate, respectively, the range of first and second force profiles for the rinsed DPPC system across pure (liposome-free) water, taken from [41].

This scenario of liposome adsorption and subsequent rupture and bilayer formation at high pressures is further strengthened by the appearance of the optical fringes at contact, as shown in the inset of figure 3, and reproduced in figure 4 which shows a schematic of what may be happening. Initially, at separations D ≈ 18 nm, the shape of the fringes indicates regions of different thickness within the contact zone (figure 4, left). This is an indication that the confined layers are not uniform, rather the surface is partially covered by liposomes and partially by bilayers (figure 4, left bottom). By following with time the shape change of the fringes, as they are further compressed, the process of transformation from liposomes to bilayers is revealed, as the fringes progressively become smooth and flat (figure 4, right). Excess material is squeezed out and the entire contact area 'thins' to D ≈ 8.5 nm, indicating that liposomes fused to form a continuous stable bilayer on each surface.

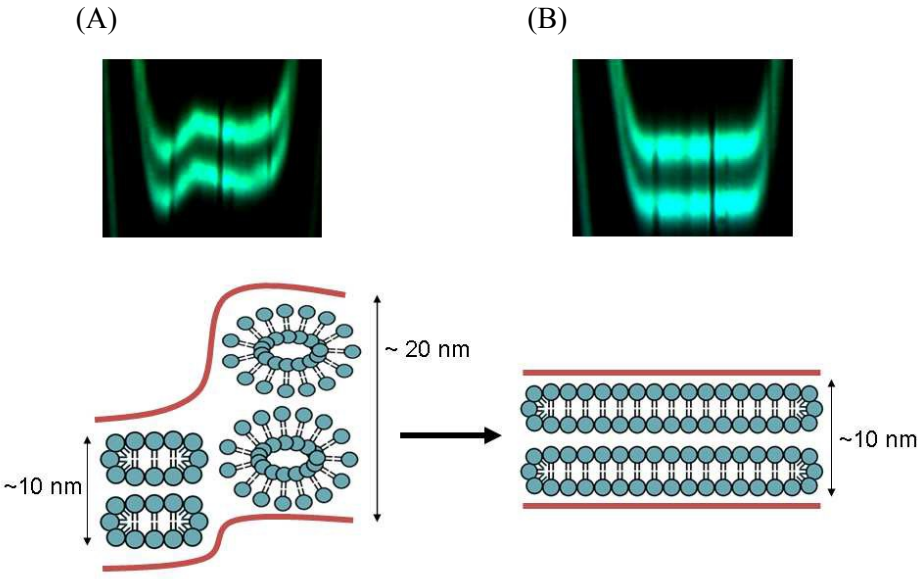

Figure 4: Schematic illustration (not to scale) of the surface layers corresponding to the different FECO fringe patterns. In (A), thickness variations are observed across the contact zone in the FECO fringe pattern, corresponding to both bilayer patches and liposomes on the surface. (B) Upon further application of pressure, an increase from 130 to 147 atm, the fringes flatten and the distance between the surfaces at this pressure, as measured from the FECO fringes, is 10±1nm. The layer thickness and the smoothness of the fringe indicates that a smooth bilayer is attached to each mica surface. This probably results from opening up of the liposomes at this higher pressure to result in a continuous bilayer, while excess material leaves the surface as previously described in [68].

Force profiles of adsorbed DPPC-SUVs measured across (liposome-free) water from a previous study [41] are overlaid in Figure 3 for comparison. In the previous study, second or subsequent approaches to contact (upper shaded band) were characterized by higher steric repulsion compared to first approaches, as a result of damage to the surface layers during shear. In the current study, (performed in liposome dispersion), however, there is no difference in the normal force profiles between the various contact positions or between first and subsequent approaches: the DPPC surface layers are robust and there is no indication of damage to the layers after the first run of approach and shear.

We next examined the normal force profiles between two mica surfaces across DSPC-SUV dispersion (figure 5). There is little scatter of the profiles, as well as no significant difference between first and subsequent approaches, up to high pressures (P ≈ 180 atm). The shape of the optical fringes at the highest pressure applied (180 atm), indicates coexistence of two different separations across the compressed contact area: one of 12±1, and the other of 21±3nm, as shown in the inset to figure 5. This might indicate partial rupture of the liposome layer at the contact position, as previously discussed and illustrated in figure 4. The range of the force profiles for the adsorbed DSPC SUVs in a pure (liposome free) water system is shown in the shaded band. It can be seen that the force profiles taken across the bulk liposome dispersion has shifted about 20nm inward compared with the liposomes free system. A possible explanation of this reduced range of steric repulsion is that in the liposome-free aqueous environment the adsorbed layers are less well-able to 'anneal', while the presence of liposomes in the surrounding dispersion facilitates such annealing, thereby forming a more uniform layer (in some analogy to annealing of adsorbed polymer layers in a polymer solution [69]).

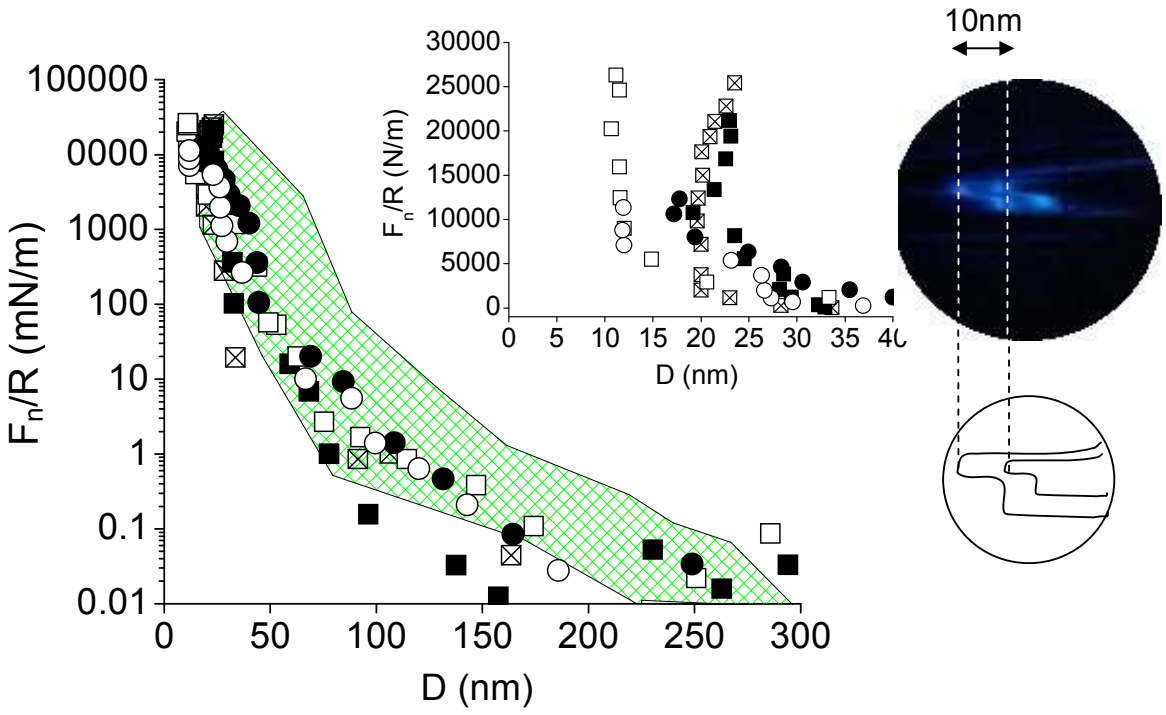

Figure 5: Typical force $F_n(D)$ versus distance D profiles between mica surfaces across a DSPC SUV dispersion, normalized as $F_n(D)/R$. D = 0 separation is defined with respect to mica-mica contact in air. Filled symbols indicate first approach to contact and empty symbols are the corresponding second approach. Shaded area shows the range of force profiles for the DSPC SUV system in pure water, reported in [41] Insets show an extended scale at close separations, final distance 21±3 nm for first approach to contact and 12±1nm for a corresponding second approach to contact, and the image of optical fringes at contact, as well as a sketch of the fringe shape. As in figure 4, the fringe shape indicates different layer thickness across the contact zone, attributed to the surface being covered by both bilayers and liposomes.

Friction forces

Typical traces of applies lateral motion, $\Delta x_0(t)$, (top zig-zag trace) vs. lateral shear forces, $F_s(t)$, (lower traces) between the SUV-coated mica surfaces across the different SUV-dispersions are shown in figure 6. Very low friction forces, close to the noise level, are recorded for POPC at all applied pressures, figure 6(A). It can be seen that in the DMPC case, figure 6(B), there is an abrupt change from a very low friction force at p=76 atm (within the scatter of the data) to very high friction, arising from a small change in the applied pressure (at p=80 atm). This high friction is manifested as rigid coupling of the surfaces as the top one is moved laterally, meaning that the surfaces move in tandem and do not slide. "Rigid coupling" is an indication

that the maximal applied shear force between the surfaces, $K_s\Delta x_{0,max,}$ was lower than the static friction force, F_s, and so could not induce sliding of the upper surface past the lower one. In the DPPC case, figure 6(C), however, as well as the DSPC case, figure 6(D), there is a gradual increase in the friction force with the increase in the applied pressure, and sliding occurs up to the highest pressures applied (>150atm).

The lubrication behavior of the POPC-SUV and DMPC-SUV systems is very different from that of the DPPC-SUV and DSPC-SUV ones. It can be seen that at almost all loads in the applied range, the friction force values are very low, and indeed not far above the detection limit δF_s of our system ($\delta F_s \approx 1\mu N$). When the pressure exceeds P ≈ 90 atm (80 atm in figure 6(B)), the friction force abruptly increases and "rigid coupling" of the surfaces is observed for DMPC, but not for POPC.

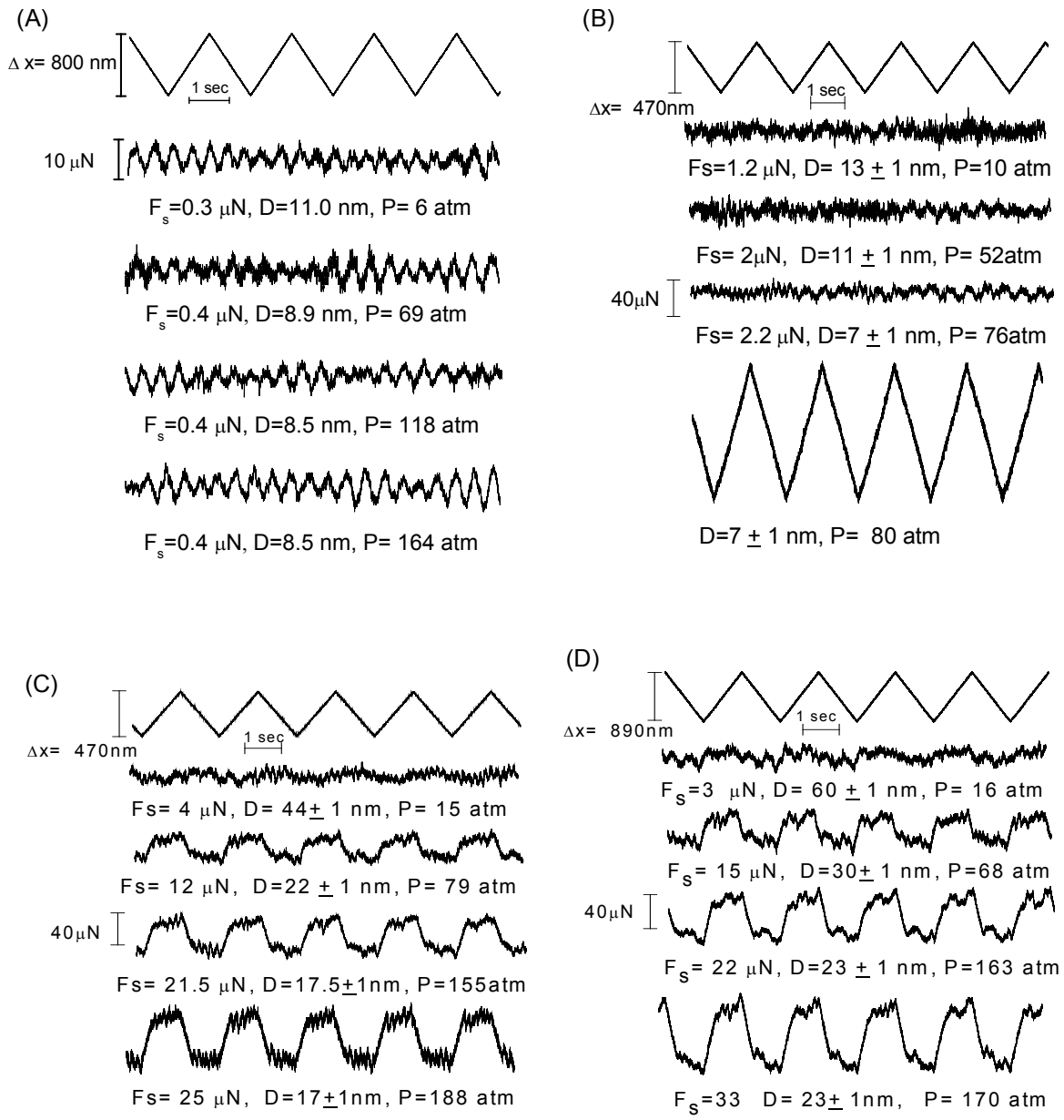

Figure 6: Typical shear traces for (A) POPC SUVs (B) DMPC SUVs (C) DPPC SUVs and (D) DSPC SUVs, each one in the corresponding SUV dispersion at 3 mM concentrations.

Similarly to our previous work (ref. [41]), in the experiments presented in this work we have examined the lubrication properties of the PC-SUV-coated surfaces at longer sliding times. As each shear profile, as shown for example in Figure 6, usually takes less than 30 seconds, prolonged shear was applied for up to one hour during several profiles, with each of the different lipid systems. It was discovered that the frictional forces either remain very low, or decrease slightly as a result of prolonged shear under pressure for all types of lipids.

Supplementary figure S1 depicts shear traces demonstrating significant reduction in the friction force following prolonged friction of 40min for the DPPC system. Similar reduction of the friction force as a result of prolonged shear was previously observed (ref. [41]).

Figure 7 summarizes the friction force versus normal load behavior for the four different systems. The detailed plots are shown in figure 7(A), where representative data sets are shown for each system. As the data for the DPPC and DSPC systems is somewhat scattered, it is shown, for clarity, as shaded bands in figure 7(B). The borders of the shaded bands are defined by linear fitting to the highest and lowest data sets of each system. For the DPPC system, there is an initial sharp increase in the friction force that is followed by further increment in the friction force and a reduction in the friction coefficient (μ= friction force/ normal load); on initial rise in F_s, $\mu=1.5\pm1\times10^{-3}$ and at higher normal loads there is a significant, one order of magnitude reduction in the friction coefficient to 1.6×10^{-4}-3.2×10^{-4} (these are the slopes of the limiting borders of the shaded band for the DPPC system). The transition does not correlate to a specific change in the spacing between the surfaces or a change in the appearance of the fringes, though it most likely results from a change to a more favorable organization of the surface layers on progressive sliding that is responsible for a reduction in the frictional energy dissipation. The same behavior is observed for the DSPC system, where initially $\mu\sim10^{-3}$, while at higher loads μ decreases to 2.4×10^{-4}-3.8×10^{-4}. For both the DPPC and the DSPC cases, the initial rise in friction as the surface approach – low load region – is likely due to the presence of excess liposomes between the surfaces, arising from their presence in the surrounding dispersion, which disappears at higher loads and shear as this excess is squeezed away. In our previous study performed in pure water [41] there was large variation between different contact positions for the DPPC system, where only 20% of the contact points measured exhibited efficient lubrication, and on first approach only, which was attributed to the marginal stability of DPPC surface layers at these conditions [41]. In the current study, in strong contrast, there is no significant difference in the friction forces measured at different contact positions or between first and subsequent approaches for the DPPC system. For a clearer comparison with our earlier study where no lipid reservoir was present (in the form of SUV dispersions) we now in fig 7B indicate frictional behavior for DMPC, DPPC and DSPC from our previous study, showing that while μ for DPPC, DSPC remains roughly similar in the presense of the dispersions, the DMPC lubrication is far more superior in the present study where self healing is possible.

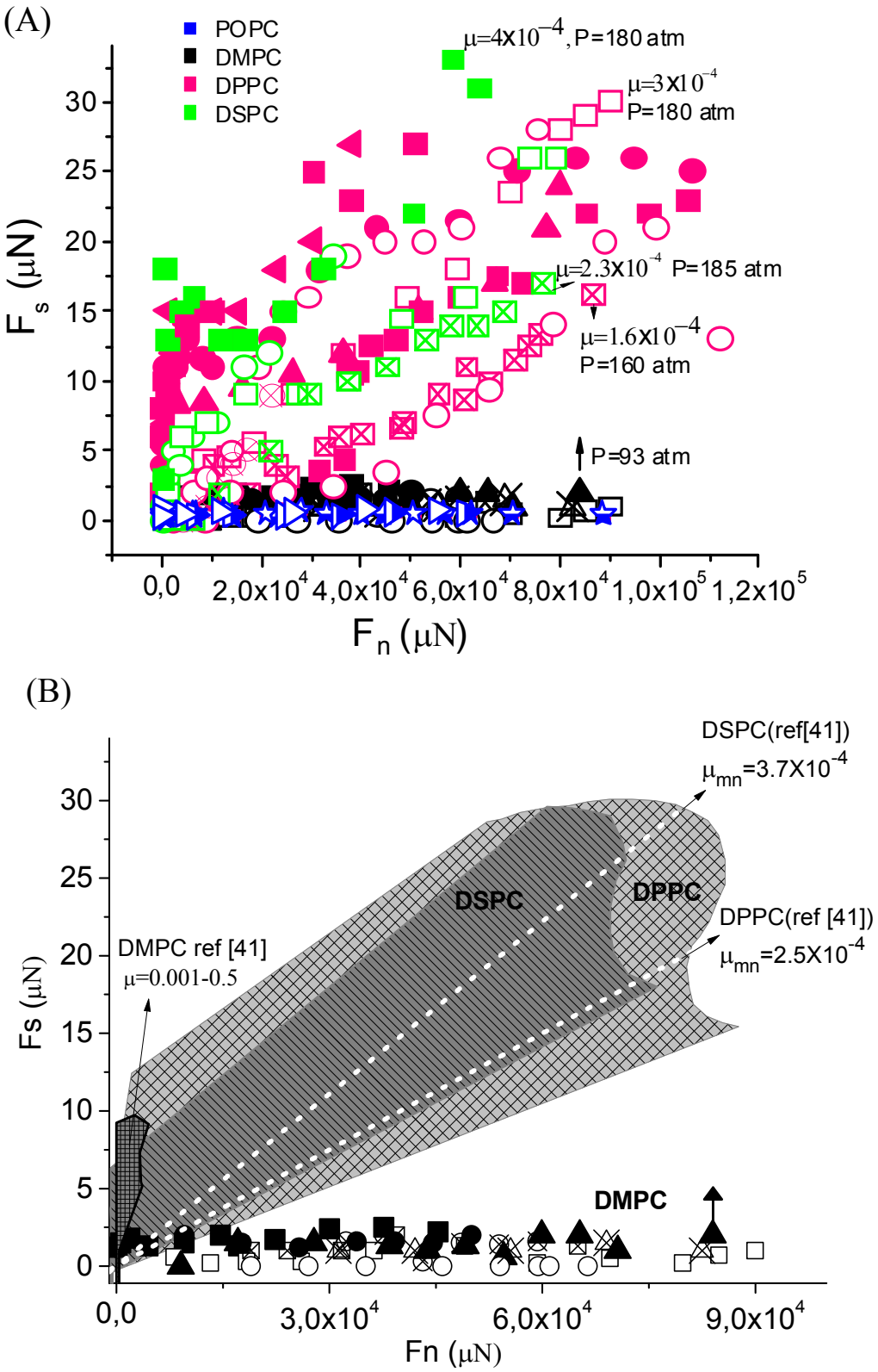

Figure 7: Summary of the friction force vs. normal load for POPC, DMPC, DPPC, and DSPC SUVs measured in the corresponding SUV dispersion at 3 mM concentration. In (A) the actual representative experimental data is shown. For clarity not all data points of all measurements are shown. Some characteristic values μ at the highest contact pressures P are given for 4 of the

DPPC, DSPC runs, as shown. In (B) the borders of the shaded bands are defined by linear fitting to the most extreme data sets of DPPC and DSPC systems as shown in (A). For both POPC and DMPC the friction force remains extremely low throughout the experiment, $\mu<10^{-4}$. Also indicated as white broken lines are the means of the extreme values of μ measured for DPPC and DSPC in ref. [41]. Likewise, the band around $Fn\sim10^{-3}$ μN indicates the behavior of DMPC from ref. [41], where the friction diverged due to damage at higher loads. Filled symbols indicate first approach to contact and empty symbols are the corresponding second approach. The arrow pointing upward corresponds to the maximum load at which the surfaces jumped into adhesive contact, at which point the friction increased abruptly and the applied force was no longer sufficient to overcome the static friction at our experimental conditions.

As can be clearly seen in figure 7, bilayers of POPC and DMPC provide better lubrication - at least up to pressures of ca. 100 atm - compared with surfaces coated by DSPC and DPPC SUVs ($\mu<10^{-4}$). This is unexpected in the light of our previous results on lubrication by PC liposomes of varying acyl chain length measured in pure water [41] where the lubrication efficiency at high pressures improved with increasing chain length. This was attributed to the increased robustness of the vesicular structure. When dispersed liposomes are present as in the current study, however, the situation is different. In order to better understand the origin of this difference, we examined the effect of pressure and shear on the morphology of DMPC bilayers immersed in DMPC SUV dispersion. This was done using an AFM tip as below.

Figure 8(A) is a tapping mode AFM scan of a freshly cleaved mica surface, immediately following immersion into DMPC-SUV dispersion, revealing a bilayer surface with some holes. In order to examine the effect of pressure and shear on this bilayer, we carried out the following: 1. Initial scan in tapping mode of a 3x3 μm area (figure 8(A)). 2. A subsequent scan in contact mode of a 1x1 μm area in the middle of the previously scanned, 3x3 μm, area (as marked by a red square in figure 8(A)). This scan is at a load of 50nN, in order to "rub" the surface and examine the effect of the rubbing on the surface morphology. 3. Another 3x3 μm area scan in tapping mode to examine the surface morphology following "rubbing" (figure 8(B)). In this post "rubbing" scan, a smooth, hole free 1x1μm area was surprisingly observed in the middle of the bilayer (figure 1(B)) (We note this square is no longer precisely positioned in the middle due to thermal drift in the instrument). It seems, therefore, that in the presence of DMPC-SUVs in the surrounding medium, the normal and shear forces applied, while scanning in contact mode, lead to healing of the layers and filling in of the previously observed holes in 1(A). In contrast, if following adsorption of the DMPC-SUV the sample is rinsed and scanned

in tapping mode (figure 8 (C)), then scanned in contact mode with 50nN force over a square where holes are present (white square in fig. 8(C)), and subsequently scanning in tapping mode (figure 8 (D)), little change in the surface morphology is revealed, unlike the previous example in 8(A) and 8(B). So, clearly, the presence of SUVs in the dispersion enables the healing of the layers when they are rubbed by the AFM tip, presumably by providing a reservoir of lipids available to fill in the holes as the layer is perturbed. As the tip perturbs the layer, it enables rapid access of DMPC lipids from the bulk reservoir (at the c.m.c.) to fill in the holes in the bilayer.

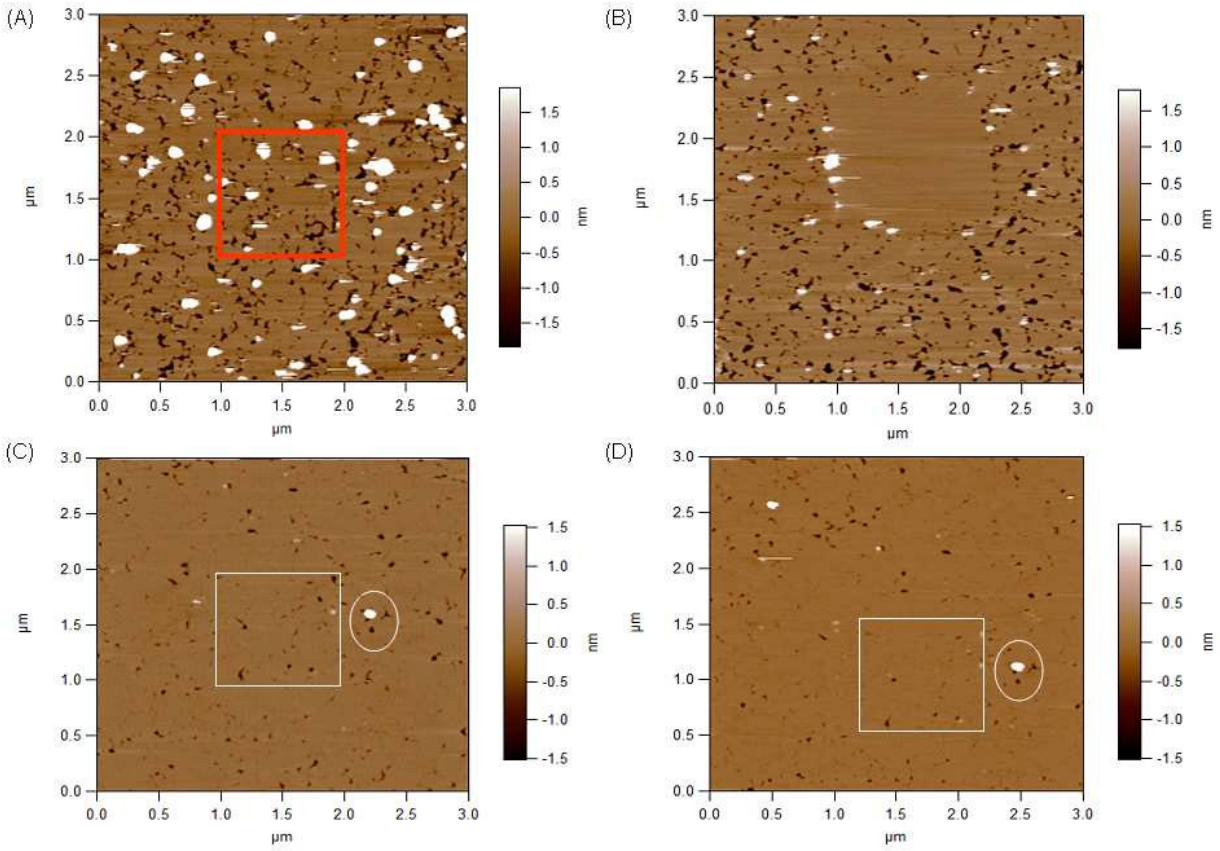

Figure 8:

AFM images of mica under 0.3mM DMPC liposome dispersion. (A) Scan in AC (tapping) mode in dispersion showing some holes as well as white blobs of excess material. (B) Scan in AC mode in dispersion, after scanning at contact mode at 50nN load was performed at the area marked in a red box in (A). A flattened hole-free square is clearly observed. (C) The same sample as in (A) and (B), after rinsing with 300ml of water, scanned in pure water. (D) The same sample after scanning in contact mode at 50nN over the area marked by a box in (C). Roughly the same area is scanned in (D), the displacement resulting from lateral surface drift.

It is seen that the holes that appear in C are not removed by the contact mode scan. Identical element are marked (by ellipses) in both images for alignment.

When a patchy DSPC bilayer surface is formed and similarly rubbed in the presence of DSPC liposomes, the contact mode rubbing does not result in a smooth bilayer (as for DMPC), even upon continuous scanning for one hour. This difference between DMPC and DSPC self healing is likely due to the timescales involved. The timescale for DMPC SUVs adsorption and rupture on a mica or silica surface is on the order of minutes at most[41, 70] , while DSPC SUVs should take ~3000 times longer to rupture [41], as seen in the following rough estimate of the relative stabilities of the SUVs. For each two additional $-CH_2-$ group on a PC tail there is an additional interaction energy $\delta\varepsilon = \alpha k_B T$ say, required to disrupt the liposome. This arises from hydrophobic interactions, modulated by some difference in hydration energies of the neighboring hydrated phosphocholine headgroups (since the longer tailed bilayers will have a higher areal density of headgroups [71]. Thus one requires roughly $\Delta E \approx 4\delta\varepsilon \approx 4\alpha k_B T$ additional energy to disrupt the DSPC-SUVs relative to the DMPC-SUVs bilayers. The magnitude of $\delta\varepsilon$ for the disruption process is not precisely known, but may be estimated from the properties of the liposomes, in particular data on the relative critical micelle concentrations of liposomes with different acyl chain lengths, which would suggest $\alpha \approx 2$ [41, 72] Thus $\Delta E \approx 8k_B T$. If we assume a simple Eyring transition-state model [73] to describe the rupture process, with mean time $\tau_{rupture}$(PC) for rupture of an SUV bilayer, then we might expect $\tau_{rupture}(DSPC) \approx \tau_{rupture}(DMPC) \times e^{\Delta E/k_B T} \approx (3x10^3)\tau_{rupture}(DMPC)$. We also note that the bending energy of DSPC is higher than that of DMPC [1, 74], therefore DMPC liposomes should more easily deform and accommodate the structures of the layer defects. While these estimates are for rupture of SUVs rather than for healing, we would, by analogy, expect dynamic processes in general to be much faster for the shorter (DMPC) or less ordered (POPC) acyl-chain lipids.

We may, therefore, attribute the differences between POPC or DMPC vs DPPC or DSPC to the difference in their surface morphology; the POPC and DMPC liposomes rupture and fuse on adsorption on the mica surface to form a continuous lamellar phase (figure 8). The DPPC SUVs are initially in a vesicular shape, and may rupture under load during the SFB experiment. The DSPC SUVs remain as vesicles under load as well, at least partially, as we learn from the morphology of the fringes (see inset to figure 5). The optical fringes indicate coexistence of regions of different thickness, corresponding to both bilayers (ca. 10nm, i.e. a 5nm bilayer on each surface) and liposomes (ca. 20nm, a flattened liposome consisting of two bilayers on each surface) within the contact zone. Upon compression and shear of the surfaces, the more

uniform and smooth surface of continuous bilayers exhibits reduced friction compared with the liposome covered surface. The vesicle covered surface is more heterogeneous, hence there is a larger scatter in the friction coefficients for the DPPC and DSPC systems. An analogous effect of different surface layer morphology on lubrication performance was observed with surfactants, where smooth bilayers lubricated better then cylindrical aggregates [75]. This was attributed to additional dissipation that may result due to viscoelastic effects as the rodlike surface micellar structures are forced past each other [75].

In addition to the difference in morphology between POPC or DMPC vs DPPC or DSPC SUVs, there is also advantage to the POPC and DMPC due to their more rapid healing. The short timescales for healing of POPC and DMPC bilayers enable maintaining of smooth, continuous bilayers. POPC and DMPC can rapidly recover between the compression and shear cycles, enabling reproducible and low friction for subsequent approaches to contact. This is consistent with higher lateral diffusion coefficients, at room temperature, of mica-supported DMPC bilayers compared with DPPC bilayers [76]. This idea is also further supported by a comparative AFM study of DLPC (12:0) and DSPC bilayers in water, which demonstrated that the liquid-disordered (LD) phase DLPC (12:0) can very quickly (up to minutes) recover after indentation with an AFM tip, unlike DSPC [77]. So overall, the softer and more mobile lipids, POPC and DMPC, result in a rapidly self-healing surface layer on the mica surface, which provides a uniform and smooth interface. We note however that the presence of liposomes/lipids in the surrounding medium also improves the nature of the DPPC layers, which had only marginal lubrication efficiency in pure water [41]

In summary, for the lipid systems considered, there is interplay of different factors affecting the boundary lubrication: robustness of the boundary layer, its uniformity and smoothness, its ability to heal, and the hydration level of the exposed phosphocholine groups. When considering the series of lipids DMPC, DPPC, DSPC, as the length of the acyl chain is increased, the layers are more robust and stable on the surface. This is because each additional –CH2- group in the acyl tails is associated with an additional binding energy (to neighboring tails) of a little under kBT [78]. This is also discussed more quantitatively in ref. [41] where the stability to rupture of DMPC-SUVs is compared to that of DSPC-SUVs. On the other hand, as the chains are more densely packed, the headgroup area decreases [71, 79], resulting in more headgroups/unit area. This nonetheless leads to impaired hydration lubrication, which we attribute as follows: The more compact configuration of phosphocholine headgroups in the case of the more densely-packed lipids (longer acyl chains) is likely to be associated with a

significantly reduced level of hydration per headgroup, which more than counters the effect of larger headgroup areal density. Thus the number of hydration water molecules per unit area is reduced, leading to a lower overall efficiency of the hydration lubrication. For the liquid phase POPC lipids, the head-group area is also larger than in the more ordered gel phase, likely enabling enhanced hydration lubrication due to the larger hydration shell [63]. In the absence of a lipid reservoir, the surface layer robustness is essential for enabling efficient lubrication, as seen in our previous study [41]. However in the presence of a lipid reservoir, the softer layers can self-heal and the robustness plays a less crucial role. Under these conditions, the hydration level of the lipid headgroups plays the more important role in enhancing lubrication via the hydration lubrication mechanism. This is in line with our previous observation of sliding between uniform layers of DPPC-SUV compared to DSPC-SUV, where (on a first approach to contact prior to layer degradation) the DPPC exhibited a lower friction coefficient attributed to its better hydration [41]. In other words, where self-healing of the more hydrated headgroups (DMPC, POPC) is possible, they act as better lubricants. Where it is not possible- as in our earlier study- it is the more robust PC's (DPPC, DSPC) that are superior lubricants at high pressures (where the less robust DMPC, POPC undergo irreversible damage.)

Conclusions

Our previous studies on lubrication by rinsed liposome layers showed that their robustness, as reflected in their increasing acyl chain lengths, DSPC>DPPC>DMPC, provided the most important contribution to their lubrication performance; essentially, the deeper the lipid was in its solid phase, the more robust and better lubricating its vesicles. The present study of these lipids, as well as the LD phase POPC, in the presence of their corresponding SUV dispersions revealed an unexpected reversal in the trend, as now DMPC and POPC provide superior lubrication to that of DPPC and DSPC (which is also very good for these lipids, but characterized by slightly higher friction coefficients). This is attributed to fast self healing of the softer surface layers (which are in their liquid disordered phase, POPC, or close to it, DMPC), which renders the robustness of the DPPC or DSPC (both in their solid ordered phase) less important at these conditions. DMPC layers were able to provide reversible and reproducible lubrication with extremely low friction ($\mu<10^{-4}$) up to pressures of 70-90 atm, and POPC layers exhibited similarly low friction ($\mu<10^{-4}$) up to pressures as high as 160 atm. Under these experimental conditions, the enhanced hydration of the less-densely packed POPC and DMPC surface layers now plays an important role, and allows enhanced lubrication via the hydration lubrication mechanism. Their more uniform and smooth surface morphology may

provide an additional advantage. These insights may have practical implications wherever lubrication in aqueous media is at a premium.

Acknowledgements:

We thank the European Research Council (ERC Advanced Grant HydrationLube), the Charles McCutchen Foundation, the Israel Science Foundation through the ISF-NSFC programme, the Minerva Foundation and the American Chemical Society (ACS-PRF # 55089-ND10) for support of this work. This work was made possible in part through the historic generosity of the Harold Perlman Family.

References

1. Mouritsen, O.G., *Life - as a matter of fat the emerging science of lipidomics*. Frontiers collection. 2005, Springer: Berlin.
2. Hills, B.A., *Surface-active phospholipid: a Pandora's box of clinical applications. Part II. Barrier and lubricating properties.* Internal Medicine Journal, 2002. **32**(5-6): p. 242-251.
3. Hills, B.A. and B.D. Butler, *Surfactants Identified in Synovial-Fluid and Their Ability to Act as Boundary Lubricants.* Annals of the Rheumatic Diseases, 1984. **43**(4): p. 641-648.
4. Hills, B.A. and I.M. Schwarz, *Surface-active phospholipid as the lubricating component of lubricin.* British Journal of Rheumatology, 1998. **37**(1): p. 21-26.
5. Freeman, M.A.R., T.D. Little, and S.A.V. Swanson, *Lubrication of synovial joints - possible significance of fat.* Proceedings of the Royal Society of Medicine-London, 1970. **63**(6): p. 579-&.
6. Kirk, T.B., A.S. Wilson, and G.W. Stachowiak, *The morphology and composition of the superficial zone of mammalian articular-cartilage.* Journal of Orthopaedic Rheumatology, 1993. **6**(1): p. 21-28.
7. Prete, P.E., A. Gurakarosborne, and M.L. Kashyap, *Synovial-fluid lipids and apolipoproteins - a contemporary perspective.* Biorheology, 1995. **32**(1): p. 1-16.
8. Ozturk, H.E., et al., *The effect of surface-active phospholipids on the lubrication of osteoarthritic sheep knee joints: Friction.* Tribology Letters, 2004. **16**(4): p. 283-289.
9. Crockett, R., et al., *Biochemical composition of the superficial layer of articular cartilage.* Journal of Biomedical Materials Research Part A, 2007. **82A**(4): p. 958-964.
10. Gale, L.R., et al., *Boundary lubrication of joints - Characterization of surface-active phospholipids found on retrieved implants.* Acta Orthopaedica, 2007. **78**(3): p. 309-314.
11. Katta, J., et al., *Biotribology of articular cartilage-A review of the recent advances.* Medical Engineering & Physics, 2008. **30**(10): p. 1349-1363.
12. Daniel, M., *Role of surface-active lipids in cartilage lubrication.* Advances in Planar Lipid Bilayers and Liposomes, Vol 15, 2012. **15**: p. 225-243.
13. Seror, J., et al., *Supramolecular synergy in the boundary lubrication of synovial joints.* Nature Communications, 2015. **6**.
14. Klein, J., *Molecular mechanisms of synovial joint lubrication.* Proceedings of the Institution of Mechanical Engineers Part J-Journal of Engineering Tribology, 2006. **220**(J8): p. 691-710.
15. Dowson, D., *Bio-tribology.* Faraday Discussions, 2012. **156**(0): p. 9-30.

16. Hodge, W.A., et al., *Contact Pressures in the Human Hip-Joint Measured Invivo.* Proceedings of the National Academy of Sciences of the United States of America, 1986. **83**(9): p. 2879-2883.
17. Morrell, K.C., et al., *Corroboration of in vivo cartilage pressures with implications for synovial joint tribology and osteoarthritis causation.* Proceedings of the National Academy of Sciences of the United States of America, 2005. **102**(41): p. 14819-14824.
18. Crockett, R., *Boundary Lubrication in Natural Articular Joints.* Tribology Letters, 2009. **35**: p. 77-84.
19. Hills, B.A., *Oligolamellar Lubrication of Joints by Surface-Active Phospholipid.* Journal of Rheumatology, 1989. **16**(1): p. 82-91.
20. Hills, B.A., *Boundary lubrication in vivo.* Proceedings of the Institution of Mechanical Engineers Part H-Journal of Engineering in Medicine, 2000. **214**(H1): p. 83-94.
21. Hills, B.A. and R.W. Crawford, *Normal and prosthetic synovial joints are lubricated by surface-active phospholipid - A hypothesis.* Journal of Arthroplasty, 2003. **18**(4): p. 499-505.
22. Ogston, A.G. and J.E. Stanier, *The Physiological Function of Hyaluronic Acid in Synovial Fluid; Viscous, Elastic and Lubricant Properties.* The Journal of Phsiology, 1953. **119**: p. 244-252.
23. Radin, E.L., D.A. Swann, and P.A. Weisser, *Separation of a Hyaluronate-Free Lubricating Fraction from Synovial Fluid.* Nature, 1970. **228**(5269): p. 377-&.
24. Seror, J., et al., *Articular Cartilage Proteoglycans As Boundary Lubricants: Structure and Frictional Interaction of Surface-Attached Hyaluronan and Hyaluronan-Aggrecan Complexes.* Biomacromolecules, 2011. **12**(10): p. 3432-3443.
25. Seror, J., et al., *Normal and Shear Interactions between Hyaluronan-Aggrecan Complexes Mimicking Possible Boundary Lubricants in Articular Cartilage in Synovial Joints.* Biomacromolecules, 2012. **13**(11): p. 3823-3832.
26. Swann, D.A., et al., *Role of Hyaluronic-Acid in Joint Lubrication.* Annals of the Rheumatic Diseases, 1974. **33**(4): p. 318-326.
27. Swann, D.A., H.S. Slayter, and F.H. Silver, *The Molecular-Structure of Lubricating Glycoprotein-I, the Boundary Lubricant for Articular-Cartilage.* Journal of Biological Chemistry, 1981. **256**(11): p. 5921-5925.
28. Zappone, B., et al., *Adsorption, lubrication, and wear of lubricin on model surfaces: Polymer brush-like behavior of a glycoprotein.* Biophysical Journal, 2007. **92**(5): p. 1693-1708.
29. Sotres, J. and T. Arnebrant, *Experimental Investigations of Biological Lubrication at the Nanoscale: The Cases of Synovial Joints and the Oral Cavity.* Lubricants, 2013. **1**(4): p. 102.
30. Hills, B.A., *Oligolamellar Nature of the Articular Surface.* Journal of Rheumatology, 1990. **17**(3): p. 349-356.
31. Jay, G.D., B.P. Lane, and L. Sokoloff, *Characterization of a Bovine Synovial-Fluid Lubricating Factor .3. The Interaction with Hyaluronic-Acid.* Connective Tissue Research, 1992. **28**(4): p. 245-255.
32. Seror, J., R. Sorkin, and J. Klein, *Boundary lubrication by macromolecular layers and its relevance to synovial joints.* Polymers for Advanced Technologies, 2014. **25**(5): p. 468-477.
33. Jay, G.D., et al., *The role of lubricin in the mechanical behavior of synovial fluid.* Proceedings of the National Academy of Sciences of the United States of America, 2007. **104**(15): p. 6194-6199.
34. Schmidt, T.A., et al., *Boundary lubrication of articular cartilage - Role of synovial fluid constituents.* Arthritis and Rheumatism, 2007. **56**(3): p. 882-891.

35. Briscoe, B.J. and D.C.B. Evans, *The Shear Properties of Langmuir-Blodgett Layers.* Proceedings of the Royal Society of London Series a-Mathematical Physical and Engineering Sciences, 1982. **380**(1779): p. 389-&.
36. Bowden, F.P. and D. Tabor, *Friction and lubrication*. 1967: Methuen.
37. Goldberg, R., et al., *Interactions between Adsorbed Hydrogenated Soy Phosphatidylcholine (HSPC) Vesicles at Physiologically High Pressures and Salt Concentrations.* Biophysical Journal, 2011. **100**(10): p. 2403-2411.
38. Goldberg, R., et al., *Boundary Lubricants with Exceptionally Low Friction Coefficients Based on 2D Close-Packed Phosphatidylcholine Liposomes.* Advanced Materials, 2011. **23**(31): p. 3517-3521.
39. Klein, J., *Hydration lubrication.* Friction, 2013. **1**(1): p. 1-23.
40. Sorkin, R., et al., *Mechanical Stability and Lubrication by Phosphatidylcholine Boundary Layers in the Vesicular and in the Extended Lamellar Phases.* Langmuir, 2014. **30**(17): p. 5005-5014.
41. Sorkin, R., et al., *Origins of extreme boundary lubrication by phosphatidylcholine liposomes (vol 34, pg 5465, 2013).* Biomaterials, 2013. **34**(37): p. 9736-9736.
42. Chen, Y., R.W. Crawford, and A. Oloyede, *Unsaturated phosphatidylcholines lining on the surface of cartilage and its possible physiological roles.* Journal of Orthopaedic Surgery and Research, 2007. **2**: p. 14-14.
43. Sarma, A.V., G.L. Powell, and M. LaBerge, *Phospholipid composition of articular cartilage boundary lubricant.* Journal of Orthopaedic Research, 2001. **19**(4): p. 671-676.
44. Sorkin, R., et al., *Origins of extreme boundary lubrication by phosphatidylcholine liposomes.* Biomaterials, 2013. **34**(22): p. 5465-5475.
45. Watanabe, M., et al., *Ultrastructural study of upper surface layer in rat articular cartilage by "in vivo cryotechnique" combined with various treatments.* Medical Electron Microscopy, 2000. **33**(1): p. 16-24.
46. Crockett, R., et al., *Imaging of the the surface of human and bovine articular cartialge with ESEM and AFM.* Tribology Letters, 2005. **19**: p. 311-317.
47. Chong, K.W., et al., *Fibroblast Growth Factor 2 Drives Changes in Gene Expression Following Injury to Murine Cartilage In Vitro and In Vivo.* Arthritis and Rheumatism, 2013. **65**(9): p. 2346-2355.
48. Watt, F.E., et al., *Src and Fibroblast Growth Factor 2 Independently Regulate Signaling and Gene Expression Induced by Experimental Injury to Intact Articular Cartilage.* Arthritis and Rheumatism, 2013. **65**(2): p. 397-407.
49. Murakami, T., et al., *Influence of synovia constituents on tribological behaviors of articular cartilage.* Friction, 2013. **1**(2): p. 150-162.
50. Wang, M., et al., *Hyaluronan and Phospholipid Association in Biolubrication.* Biomacromolecules, 2013. **14**(12): p. 4198-4206.
51. Koynova, R. and M. Caffrey, *Phases and phase transitions of the phosphatidylcholines.* Biochimica Et Biophysica Acta-Reviews on Biomembranes, 1998. **1376**(1): p. 91-145.
52. Kastelowitz, N. and H. Yin, *Exosomes and Microvesicles: Identification and Targeting By Particle Size and Lipid Chemical Probes.* Chembiochem, 2014. **15**(7): p. 923-928.
53. Vlassov, A.V., et al., *Exosomes: Current knowledge of their composition, biological functions, and diagnostic and therapeutic potentials.* Biochimica et Biophysica Acta (BBA) - General Subjects, 2012. **1820**(7): p. 940-948.
54. Robbins, P.D. and A.E. Morelli, *Regulation of immune responses by extracellular vesicles.* Nature Reviews Immunology, 2014. **14**(3): p. 195-208.
55. Matei, C.I., et al., *Ultrastructural Analysis of Healthy Synovial Fluids in Three Mammalian Species.* Microscopy and Microanalysis, 2014. **20**(3): p. 903-911.
56. Lichtenberg, D. and Y. Barenholz, *Liposomes - Preparation, Characterization, and Preservation.* Methods of Biochemical Analysis, 1988. **33**: p. 337-462.

57. Klein, J. and E. Kumacheva, *Simple liquids confined to molecularly thin layers. I. Confinement-induced liquid-to-solid phase transitions.* Journal of Chemical Physics, 1998. **108**(16): p. 6996-7009.
58. Derjaguin, B.V., Kolloidn. Zh., 1934. **69**: p. 155.
59. Raviv, U., et al., *Lubrication by charged polymers.* Nature, 2003. **425**(6954): p. 163-165.
60. Raviv, U. and J. Klein, *Fluidity of bound hydration layers.* Science, 2002. **297**(5586): p. 1540-1543.
61. Johnson, K.L., *Contact Mechanics*. 1987, Cambridge University Press.
62. Raviv, U., P. Laurat, and J. Klein, *Time dependence of forces between mica surfaces in water and its relation to the release of surface ions.* Journal of Chemical Physics, 2002. **116**(12): p. 5167-5172.
63. Leekumjorn, S. and A.K. Sum, *Molecular characterization of gel and liquid-crystalline structures of fully hydrated POPC and POPE bilayers.* Journal of Physical Chemistry B, 2007. **111**(21): p. 6026-6033.
64. Israelachvili, J., et al., *Correlation of AFM and SFA measurements concerning the stability of supported lipid bilayers.* Biophysical Journal, 2004. **86**(2): p. 870-879.
65. Vermette, P. and D. Nejat, *Liposome Characterization by Quartz Crystal Microbalance Measurements and Atomic Force Microscopy*, in *Methods in Enzymology*. 2009, Academic Press. p. 43-73.
66. Sakai, H., et al., *DSPC/DLPC Mixed Films Supported on Silica: A QCM-D and Friction Force Study.* Journal of Oleo Science, 2011. **60**(4): p. 177-183.
67. Schonherr, H., et al., *Vesicle adsorption and lipid bilayer formation on glass studied by atomic force microscopy.* Langmuir, 2004. **20**(26): p. 11600-11606.
68. Zhu, L., D. Gregurec, and I. Reviakine, *Nanoscale Departures: Excess Lipid Leaving the Surface during Supported Lipid Bilayer Formation.* Langmuir, 2013. **29**(49): p. 15283-15292.
69. Pefferkorn, E., A. Haouam, and R. Varoqui, *Kinetics of Exchange between Adsorbed and Free Polymers at a Solid Liquid Interface.* Macromolecules, 1989. **22**(6): p. 2677-2682.
70. Israelachvili, J.N., et al., *Formation of Supported Bilayers on Silica Substrates.* Langmuir, 2009. **25**(12): p. 6997-7005.
71. Petrache, H.I., S.W. Dodd, and M.F. Brown, *Area per lipid and acyl length distributions in fluid phosphatidylcholines determined by H-2 NMR spectroscopy.* Biophysical Journal, 2000. **79**(6): p. 3172-3192.
72. Marsh, D., *Handbook of Lipid Bilayers*. 2 ed. 1990: CRC Press, Boca Raton.
73. Tabor, D., *Gases, Liquids and Solids*. 2 ed. 1980: Cambridge University Press.
74. Picas, L., F. Rico, and S. Scheuring, *Direct Measurement of the Mechanical Properties of Lipid Phases in Supported Bilayers.* Biophysical Journal, 2012. **102**(1): p. L1-L3.
75. Silbert, G., N. Kampf, and J. Klein, *Normal and Shear Forces between Charged Solid Surfaces Immersed in Cationic Surfactant Solution: The Role of the Alkyl Chain Length.* Langmuir, 2014. **30**(18): p. 5097-5104.
76. Scomparin, C., et al., *Diffusion in supported lipid bilayers: Influence of substrate and preparation technique on the internal dynamics.* European Physical Journal E, 2009. **28**(2): p. 211-220.
77. Goertz, M.P., et al., *Nanomechanical Contrasts of Gel and Fluid Phase Supported Lipid Bilayers.* Journal of Physical Chemistry B, 2009. **113**(27): p. 9335-9339.
78. Israelachvili, J.N., *Intermolecular and Surface Forces.* (3rd ed). Elsavier, USA, 2011
79. Balgavy, P., et al., *Bilayer thickness and lipid interface area in unilamellar extruded 1,2-diacylphosphatidylcholine liposomes: a small-angle neutron scattering study.* Biochimica Et Biophysica Acta-Biomembranes, 2001. **1512**(1): p. 40-52.

In the presence of a lipid reservoir, softer lipid layers can self heal and provide enhanced lubrication via the hydration lubrication mechanism.

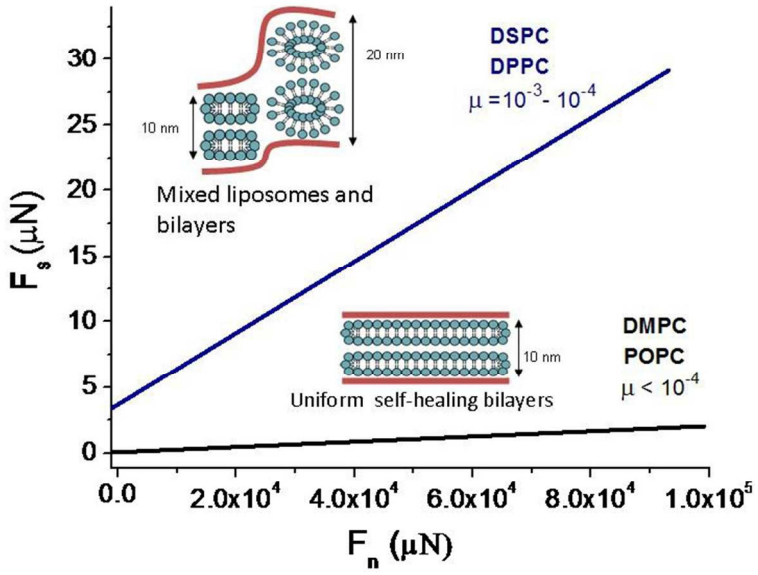

254x190mm (96 x 96 DPI)